

Aerosol optical depth retrieval from visibility in China during 1973–2014



Zhaoyang Zhang ^{a, b}, Weiling Wu ^c, Jing Wei ^{d, g}, Ying Song ^e, Xiaotong Yan ^a,
Lidong Zhu ^{a, *}, Quan Wang ^{f, **}

^a College of Geography and Environmental Sciences, Zhejiang Normal University, Zhejiang Province, China

^b Department of Land Surveying and Geo-Informatics, The Hong Kong Polytechnic University, Kowloon, Hong Kong

^c Chinese Academy for Environmental Planning, Beijing, China

^d College of Urban and Environmental Sciences, Peking University, Beijing, China

^e Quzhou Environmental Monitoring Center, Zhejiang, China

^f Faculty of Agriculture, Shizuoka University, Shizuoka 422-8529, Japan

^g College of Geomatics, Shandong University of Science and Technology, Qingdao China

HIGHLIGHTS

- An improved algorithm was developed to retrieve AOD from visibility.
- SVD method was used to investigate consistency of spatial-temporal variations.
- The spatial patterns for inferred AOD and MODIS datasets also agree very well.
- Inferred AOD can be used to better understand aerosol effects on climate change.

ARTICLE INFO

Article history:

Received 22 May 2017

Received in revised form

11 August 2017

Accepted 3 September 2017

Available online 6 September 2017

Keywords:

Visibility

Aerosol Optical Depth

Singular Value Decomposition (SVD)

Spatio-temporal variability

ABSTRACT

Visibility is a widely-used indicator to quantify aerosol loadings. However, there are still some uncertainties in retrieving Aerosol Optical Depth (AOD) from surface visibility data. In this study, a new method, KM-Elterman method, was developed to retrieve AOD based on visibility from 1973 to 2014 and MODIS (Aqua) AOD product from 2002 to 2014. The analysis indicated that KM-Elterman method performed better than previous algorithms, such as Qiu, Elterman, and M-Elterman algorithms. The correlation between inferred AOD and MODIS measurements from 2002 to 2010 reached at 0.942 and the Root Mean Squared Error (RMSE) is about 0.077 for annual inferred AOD. Singular Value Decomposition (SVD) method was used to investigate the consistency of spatio-temporal variations between inferred AOD and MODIS measurements from July 2002 to December 2014. The correlation between Principal Components (PCs) is well above 0.72. The spatial patterns of inferred AOD agreed well with that of MODIS datasets. Long-term AOD trends over China during 1973–2014 were analyzed using the inferred AOD and our results pointed out that rapidly increasing trends of AOD were observed before 1980 in North China Plain (NCP), Yangtze River Delta (YRD), central China, Sichuan Basin (SB), and Pearl River Delta (PRD). Slight decreasing trends were found in southwest China. The inferred AOD can be used to explore aerosol effects on climate change and Earth's radiative budget.

© 2017 Elsevier Ltd. All rights reserved.

1. Introduction

Aerosol particles can directly affect the Earth's solar radiation through scattering and absorbing solar radiation. Aerosols affecting the climate system still represents one of the largest uncertainties in climate studies (Field et al., 2014). Therefore, variations of aerosol loadings are essential and critical to climate change research

* Corresponding author.

** Corresponding author.

E-mail addresses: zhulidong@zjnu.cn (L. Zhu), wang.quan@shizuoka.ac.jp (Q. Wang).

(Boucher et al., 2013; Stocker, 2014). Aerosol Optical Depth (AOD) is a fundamental optical property derived from ground-based sun photometers and space-borne satellites, and it can be used to quantify aerosol loadings (Li, 2009). Thus, study of long-term AOD variability is essential to understand the aerosol effects on climate change and Earth's radiation budget. Ground-based sun photometers and satellite sensors are two main methods to monitor aerosol properties. AErosol RObotic NETwork (AERONET) is a world-wide federated sun photometer network for aerosol monitoring (Holben et al., 1998). Observations from AERONET are usually considered as reference data. In recent few years, satellite sensors have demonstrated promising accuracies in the retrieval of global AOD and the operational AOD products have been widely used in various aerosol and climate-related studies (Kaufman et al., 2005; Huang et al., 2009; Zhang and Reid, 2010; Zhang et al., 2016b).

However, most of satellites and ground-based sensors observed the AOD after 2000. Long-term AOD observations exceeding 40 years are really lack, which seriously limited the analysis of the climate effects of aerosols. Atmospheric visibility is a good indicator of air quality (Baumer et al., 2008) and has been measured for many decades at many ground meteorological stations. Retalis et al. (2010) and Zhang et al. (2016a) demonstrated that visibility can generally represent the inter-annual MODIS measurements. Elterman (1970) developed relationships between surface particle matter and vertical attenuation by deriving an exponential decrease of aerosols with height. Qiu and Lin (2001) derived AOD from visibility by correcting Elterman method to reflect the difference of surface water vapor pressure. Lin et al. (2014) employed ground-based visibility and the vertical distribution of aerosol simulated by the nested GEOS-Chem chemical transport model to infer AOD over eastern China in 2006. To overcome the disadvantage of time assuming of chemical transport model, Zhang and Wong (2017) developed a simplified algorithm using CALIPSO aerosol profile. Wu et al. (2014) improved the Elterman method by adding new parameters to reflect the difference of aerosol vertical profile. In usual, aerosol extinction coefficients at surface are common parameter to derive visibility by a simple inverse formula, named Koschmieder's equation (extinction coefficient = C/visibility) (Koschmieder, 1925). However, Koschmieder's equation can only be applied under specific atmospheric conditions (Horvath, 1971; Yuan et al., 2006; Lee et al., 2014). The range of constant in the equation is from 1.8 to 3.912 in different visibility stations for practical application (Ozkaynak et al., 1985; Yuan et al., 2006; Kessner et al., 2013). Meyer et al. (1991) illustrated that Koschmieder's equation generally underestimated the visual range using the default value. Therefore, improvement approach based on M-Elterman was proposed in this paper to derive AOD. This paper is organized as follows. Descriptions of the data, methodology are outlined in Section 2. In Section 3, the retrieval AOD from visibility and the bias between inferred AOD and satellite AOD are presented. Section 4 summarizes the discussions and conclusions.

2. Data and method

2.1. Aerosol Optical Depth data

MODerate-resolution Imaging Spectroradiometer (MODIS) Collection 6 (C6) Level 2 daily aerosol products (MYD04 for Aqua) are produced at the spatial resolution of $10\text{ km} \times 10\text{ km}$ and can be acquired from the NASA Goddard Space Flight Center. MYD04 AOD was retrieved based on three kinds of algorithms: one algorithm for ocean and two for land — the Dark-Target (DT) (Levy et al., 2010) and Deep-Blue (DB) algorithms (Hsu et al., 2004). The expected error of DT and DB AOD retrievals were within $\pm 0.05 \pm 0.15^*\text{AOD}$ (Levy et al., 2013) and $\pm 0.05 \pm 0.2^*\text{AOD}$ over land (Sayer et al.,

2013), respectively. In this paper, MYD04 combined DT and DB products between July 2002 and December 2014 were used. AOD values exceeding 2 were excluded to reduce the large uncertainties in both MODIS and visibility inferred AOD (Lin et al., 2014). The monthly data used in the retrieval method was averaged within 10 km surrounding the visibility station from daily data, while the monthly AOD used in Singular Value Decomposition (SVD) is the MODIS C6 monthly AOD products with the spatial resolution of $1^\circ \times 1$ degree. In this paper, AOD measurements between 2011 and 2014 were used to retrieve the unknown parameters in the new developed method, and the remaining data were used to validate the inferred AOD.

2.2. Visibility data

Integrated Surface Hourly Data Base (ISD) is land-based station data provided by the America National Centers for Environmental Information (NCEI). ISD consists hourly visibility data and fifty-four quality-assured algorithms of ISD were designed to eliminate obvious errors and ensure with the greatest possibility that valid values were not removed. Visibility before 1980 was recorded into ten ranks. In order to convert the data into distance, the method of Qin et al. (2010) was adopted. Visibility data after 1980 was converted to ten ranks based on recorded method before 1980. Then, average visibility can be obtained for each rank. According to the average visibility for each rank, visibility record can convert to visibility distance. Hourly visibility data were co-matched with the MODIS AOD data within ± 1 h. The visibility data were then further removed to reduce errors when the data satisfied the following conditions:

1. Corresponding relative humidity is higher than 95% (Lin et al., 2014).
2. The daily average visibility falls below one third of the values in the next and previous day (Husar et al., 2000).

3. Surface Synoptic Observations (SYNOP)

All visibility data in the station would be further excluded when it satisfied the following conditions (Husar et al., 2000):

1. The maximum visibility is below 12 km, while the median value exceeds 11 km in the station during the study period.
2. The number of non-repeating visibility values is less than five in the station during all study period.

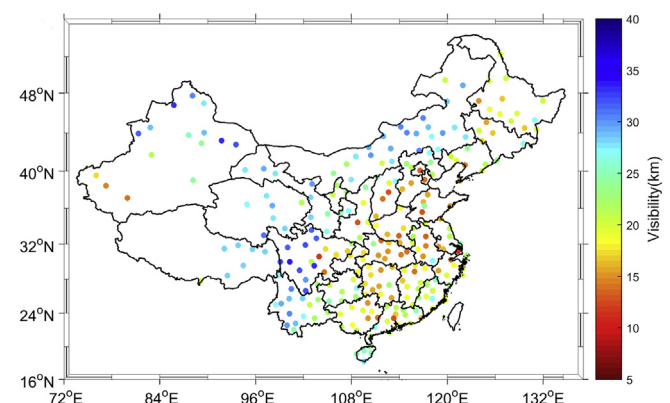


Fig. 1. Mean visibility from 1973 to 2014 at AQUA time.

3. The ratio of 75th and 50th percentile is less than 1.07 or if the ratio of the 90th to 75th percentile is less than 1.1 for a certain season.
4. If the mean and/or variance of a three-year sliding window exceed the averaged value ± 3 times standard deviation.

After some visibility data screening, coincident visibility data are available at 259 stations. The mean visibility in Aqua time between 1973 and 2014 is displayed in Fig. 1.

3.1. Retrieval method

Assuming that the impact of air molecules is neglected, the surface aerosol extinction coefficient at 550 nm is inversely proportional to surface visibility according to the Koschmieder Equation:

$$f = \begin{cases} \exp(-0.32 + 0.02V_z), & \text{Northeast of China} \\ \exp((0.42 + 0.0046p_w + 0.015V_z)\exp(-0.0047V^2/p_w)), & \text{Other regions of China} \end{cases} \quad (8)$$

$$\text{Extinction}_a = K/V \quad (1)$$

where Extinction_a represents surface aerosol extinction coefficient; K is Koschmieder constant and V is visibility from ground-based stations. In general, K depends on the contrast threshold of human eye. Errors induced by air molecules are increasing with higher visibility. Thus, the improved equation is adopted.

$$\text{Extinction}_a = K/V * (1 - V/V_0) \quad (2)$$

V_0 is the optical effects of air molecules. The aerosol extinction coefficient at height Z can be expressed as

$$\text{Extinction}(z)_a = \frac{N^A(z)}{N^A} K/V * (1 - V/V_0) \quad (3)$$

$N^A(z)$ and N^A are the aerosol particles concentrations at height z and surface, respectively. According to the equation from McClatchey et al. (1972), concentrations of aerosol particles at height z can be calculated by

$$N^A(z) = \begin{cases} 55 \exp\left[-\frac{z-5.5}{H_1}\right], & z < 5.5 \text{ km} \\ 55, & 5.5 \leq z \leq 18 \text{ km} \\ 55 \exp\left[-\frac{z-18}{H_2}\right], & z > 18 \text{ km} \end{cases} \quad (4)$$

$H_1 = 0.0222V + 0.886$ and $H_2 = 3.77 \text{ km}$ according to the research of Qiu and Lin (2001). According to the Equations (2)–(4), visibility at the height z can be expressed as

$$V_z = 3.912 / \left(0.0116 - 0.00099z + \left(\frac{3.912}{V} - 0.0116 \right) \exp\left(-\frac{z}{0.886 + 0.0222V}\right) \right) \quad (5)$$

z is the latitude of visibility station. τ_a at wavelength of 550 nm is derived using the following equation:

$$\tau_a = \left(\frac{3.912}{V} - 0.0116 \right) \left(H_1 \left(\exp\left(-\frac{z}{H_1}\right) - \exp\left(-\frac{5.5}{H_2}\right) \right) + 12.5 \exp\left(-\frac{5.5}{H_1}\right) + H_2 \exp\left(-\frac{5.5}{H_1}\right) \right) \quad (6)$$

Equation (6) is the traditional Elterman AOD retrieval method. Qiu and Lin (2001) investigated the influence of water vapor on the traditional Elterman algorithm and developed correction method to calibrate the result by dividing Chinese region into two parts. The equations in the study of Qiu and Lin (2001) are as following:

$$\tau_a = \left(\frac{3.912}{V} - 0.0116 \right) \left(H_1 \left(\exp\left(-\frac{z}{H_1}\right) - \exp\left(-\frac{5.5}{H_2}\right) \right) + 12.5 \exp\left(-\frac{5.5}{H_1}\right) + H_2 \exp\left(-\frac{5.5}{H_1}\right) \right) * f \quad (7)$$

p_w is the surface vapor pressure (unit: hPa). However, the method was only tested in 16 stations and it is hard to apply the method to the whole visibility station of China. To calibrate the effect of water vapor and aerosol profile at each station, Wu et al. (2014) adjusted some parameters in the Qiu method (Qiu and Lin, 2001) using the least squares method for each station.

$$F = \left(\frac{3.912}{V} - 0.0116 \right) \left((eV + f) \exp\left(-\frac{z}{eV + f}\right) - \exp\left(-\frac{5.5}{eV + f}\right) + 12.5 \exp\left(-\frac{5.5}{eV + f}\right) + g \exp\left(-\frac{5.5}{eV + f}\right) \right) \exp\left((a + bp_w + cV_z) \exp\left(\frac{dV^2}{p_w}\right)\right) - AOD \quad (9)$$

AOD is the measurement at the station. To further improve the accuracy of the inferred AOD, the M-Elterman method was enhanced by the following equation:

$$F = \left(\frac{h}{V} - i \right) \left((eV + f) \exp\left(-\frac{z}{eV + f}\right) - \exp\left(-\frac{5.5}{eV + f}\right) + 12.5 \exp\left(-\frac{5.5}{eV + f}\right) + g \exp\left(-\frac{5.5}{eV + f}\right) \right) \exp\left((a + bp_w + cV_z) \exp\left(\frac{dV^2}{p_w}\right)\right) - AOD \quad (10)$$

$$S = \sum_{2011}^{2014} (AOD - F)^2 \quad (11)$$

In Equation 11, S is the function of a, b, c, d, e, f, h, and i. Parameters in the equation are solved by using the extreme value principles.

$$\frac{\partial S}{\partial a} = \frac{\partial S}{\partial b} = \frac{\partial S}{\partial c} = \frac{\partial S}{\partial d} = \frac{\partial S}{\partial e} = \frac{\partial S}{\partial f} = \frac{\partial S}{\partial g} = \frac{\partial S}{\partial h} = \frac{\partial S}{\partial i} = 0$$

In this paper, monthly AOD from 2011 to 2014 were used to retrieve parameters in Equation (10) and other data were used to validate the inferred AOD in this study. The further improved retrieval method was named KM-Elterman method.

3.2. Singular Value Decomposition (SVD) method

SVD is one of the spectral techniques to separate multi-dimensional datasets into several major modes of variance. Prohaska (1976) firstly applied the Singular Value Decomposition (SVD) analysis in meteorological context to investigate the relationships between monthly sea level pressure and surface air temperature over the Hemispheric Sea and United States. The main advantage of this approach is that it can reduce data dimension and

examine both spatial and temporal variability simultaneously. In this study, the SVD method was adopted to examine the coherency between inferred AOD and MODIS measurements. Detailed information about the SVD method is as follows:

$$A = X^T Y \quad (12)$$

where X and Y represent the normalized monthly MODIS and inferred AOD from KM-Elterman, respectively. SVD method is applied on matrix M. U and V are the spatial pattern for two input parameters. U and V are obtained using equation (13).

$$A = U \lambda V^T \quad (13)$$

Time series T_x and T_y are calculated as followings:

$$T_x = XU \quad (14)$$

$$T_y = YV \quad (15)$$

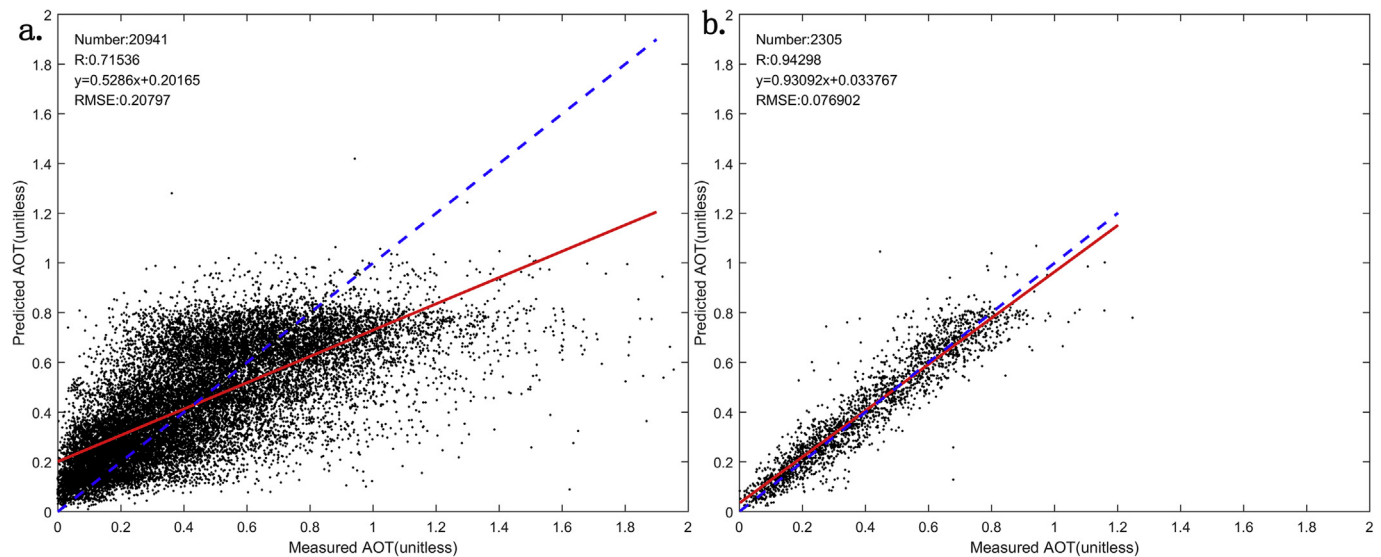


Fig. 2. Collocated comparison of monthly and annual inferred AOD from KM-Elterman method and MODIS AOD over China.

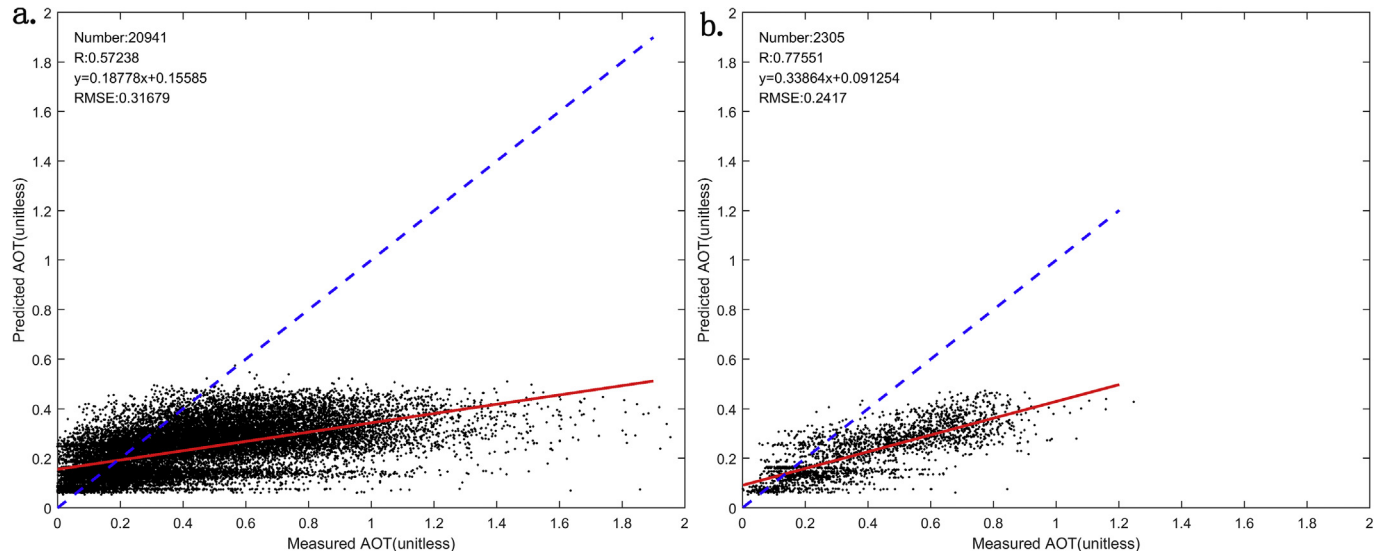


Fig. 3. Same as Fig. 2, but for Elterman method.

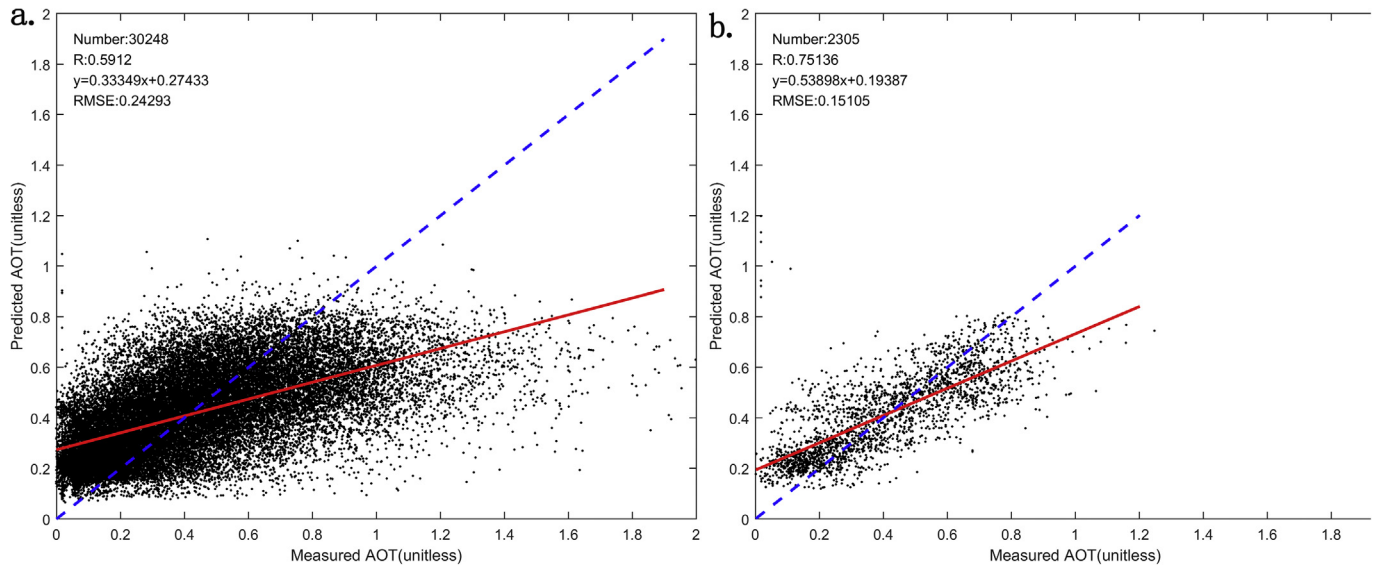


Fig. 4. Same as Fig. 2, but for Qiu method.

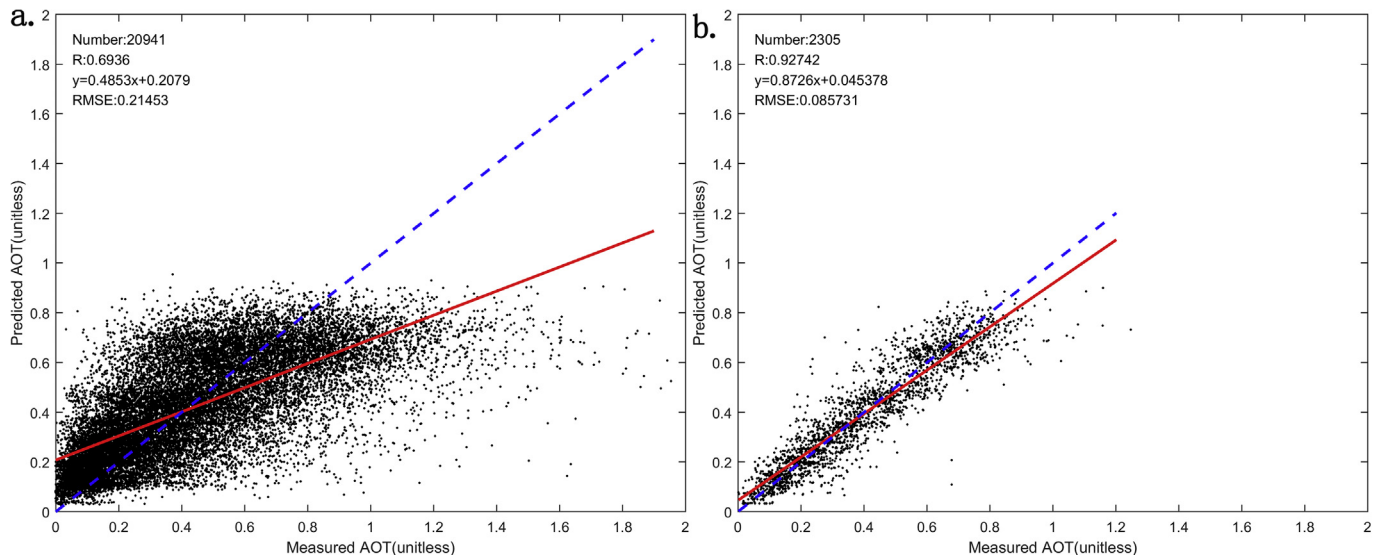


Fig. 5. Same as Fig. 2, but for M-Elterman method.

The fraction of squared covariance (SCF) explained by the i th mode is obtained using equation (16).

$$SCF_i = \lambda_i^2 / \sum_{i=1}^N \lambda_i^2 \quad (16)$$

4. Results

4.1. Evaluation of inferred AOD with MODIS AOD

The retrieved AOD from KM-Elterman algorithm is validated with MODIS AOD from 2002 to 2010. In Fig. 2, blue line represents 1:1 line and red line is the regression line. The correlation coefficient between monthly inferred AOD and MODIS measurements researches 0.715 ($N = 20941$) and root mean square error is 0.207. The scatter plot indicated that the method failed to retrieve the AOD exceeded 1. Fig. 2b shows the performance of annual inferred

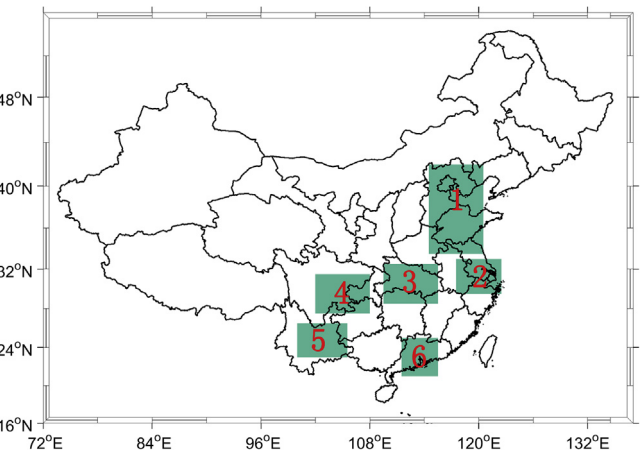


Fig. 6. Region domains defined in this paper. 1. North China Plain (NCP), 2. Yangtze River Delta (YRD), 3. Central China, 4. Sichuan Basin (SB), 5. Southwest China, and 6. Pearl River Delta (PRD).

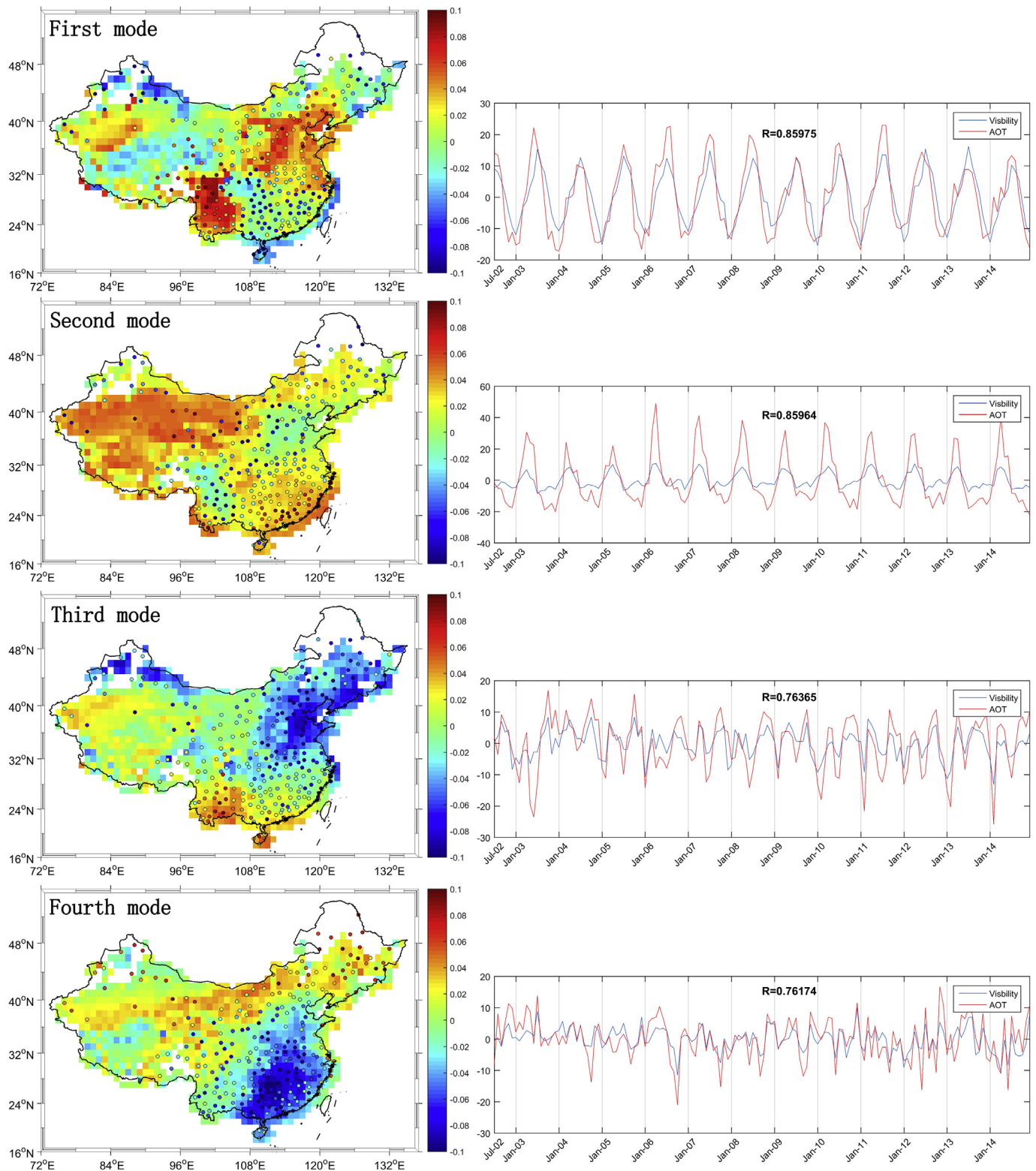


Fig. 7. The first four spatial patterns and Principal Components (PCs) of monthly inferred AOD and MODIS measurements. The legend in the spatial pattern indicates the extent of variation. Deep blue and red colors represent large variation.

AOD. The slope of regression almost coincides with the 1:1 line and the RMSE is less than 0.077, which indicated that good results were obtained when the monthly AOD was less than 1. Satisfied annual AOD were obtained by using the new developed method. To compare the new algorithm to previous methods, AOD from visibility were also calculated using Elterman (Fig. 3), Qiu (Fig. 4), and M-Elterman (Fig. 5) algorithms. Correlation coefficients between monthly inferred AOD and MODIS measurements are 0.572, 0.591, and 0.694 for Elterman, Qiu, and M-Elterman methods, respectively. Annual mean data shows better performance than monthly AOD data (0.776 for Elterman method, 0.751 for Qiu method, and 0.92 for M-Elterman method). Only RMSE in M-Elterman method is lower than 0.09. Compared to these methods, KM-Elterman method can retrieve AOD with higher accuracy over China.

In this study, SVD method was used to evaluate the spatio-temporal variability of the inferred AOD over China from July 2002 to December 2014. The first four modes of AOD data from monthly Aqua observations and inferred AOD can explain most of

the variance ($48.09\% + 35.34\% + 6.66\% + 2.96\%$) (Fig. 7). In the first mode, the correlation between PCs is above 0.85. According to the PCs of first mode, it reflects the annual variability with the maximum value in summer and minimum value in winter. The associated spatial pattern shows strong variability in North China Plain (NCP) and southwest China. Therefore, PCs of the first mode mainly represent the seasonal variability in these two regions. Similar seasonal AOD variations were also found in the research of Che et al. (2015) using the ground-based sun photometer. Luo et al. (2014) pointed out that the seasonal characteristics were influenced by Asian summer monsoons. PCs of the second mode also show annual variability but peak in spring. For the spatial patterns, both inferred AOD and MODIS data show strong signs in southeast coast and northwest China. High aerosol loadings in spring over northwest China are mainly impacted by the dust events (Che et al., 2015). Mode 3 shows the semi-annual cycle over part of NCP region, northwest China. Mode 4 captures the inter-annual variability over China. Correlations between PCs in mode 3 and 4 are higher than

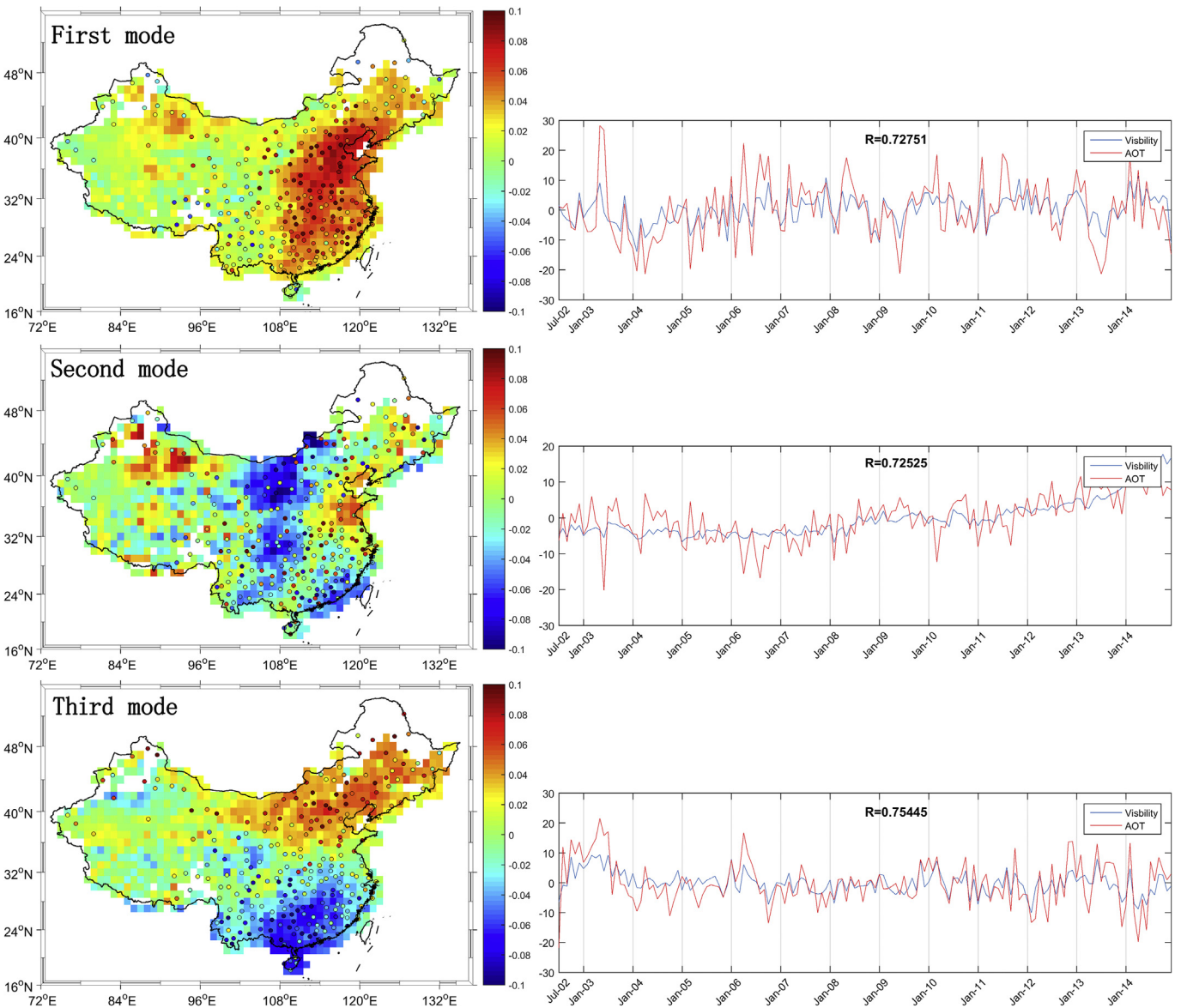


Fig. 8. The first three spatial patterns and Principal Components (PCs) of de-seasonalized inferred AOD and MODIS measurements. The legend in the spatial pattern indicates the extent of variation. Deep blue and red colors represent large variation.

0.76. In the fourth mode, strong negative signal occurs in southern China. It indicated that the corresponding PCs can reflect the inter-annual variability for southern China.

Deseasonalized datasets were also used to investigate the inter-annual variability (Fig. 8). The first three modes can capture 31.63%, 16.45%, and 12.08% of total variance, respectively. All PCs of three modes show good correlations (>0.72) between inferred AOD and MODIS AOD. The first mode represents the inter-annual variability over east China. Inferred AOD can capture the general characteristics of spatial distribution of AOD. In the second mode, spatial patterns show large variability in (region 1) Inner Mongolia, Gansu, Ningxia, (region 2) Sichuan Basin (SB), (region 3) southeast coast. Combining with PCs of the second mode, decreasing AOD trends were found in these three regions. The decreasing trends over region of Inner Mongolia, Gansu, Ningxia are influenced by the declining trend of dust storm frequency (Zhang et al., 2006). The decreasing AOD trends in SB and southeast coast might be caused by the fuel-gas desulfurization facilities in China after 2007 (Klimont et al., 2013). According to the analysis of SVD method, the inferred AOD from KM-Elterman algorithm can better reflect the seasonal and inter-annual variability.

4.2. AOD characteristics of the past 42 years

The spatial distribution of AOD is investigated for several periods of 8–10 years from 1973 to 2014 (Fig. 9). The mean AODs for four decades are 0.388, 0.396, 0.403, 0.411 and 0.414. There are 32.04% (83/259) of stations with mean AOD greater than 0.5 during 1973–1980. Most of these stations were distributed in the populated regions, such as North China Plain (NCP), Pearl River Delta (PRD), Sichuan Basin (SB) and central China. During 1981–1988, the number of stations which the AOD exceeds 0.5 reached to 88. There are 93, 95 and 97 stations with mean station AOD values greater than 0.5 during 1989–1996, 1997–2004, and 2005–2014, respectively (see Fig. 10). In the first period, increasing AOD trends were observed in 201 stations. Relative insignificant variations of AOD were shown in northeast, northwest and southwest China since the second period. Large variations of AOD were mainly located at NCP, YRD, PRD and central China in the last three periods. The AOD trends in some stations over south China decreased during 2005–2014. The result in this study was consistent with the

research from Zhang et al. (2016b). Decreasing AOD trends were related to the implementation of flue gas desulphurization in China (Klimont et al., 2013). According to the third mode, strong reversed signals were shown in northeast China and southern coast (see Fig. 8).

Six regions were selected in Fig. 6 to investigate the regional variations of AOD during 1973–2014, including North China Plain (NCP), Yangtze River Delta (YRD), central China, Sichuan Basin (SB), southwest China, and Pearl River Delta (PRD). It was observed that rapid growth of AOD dominated before 1980 over these regions, except for southwest China (Fig. 11). After 1980, increasing AOD trends from 1981 to 2014 were found in NCP, YRD, central China, and PRD, except SB. In this period, maximum aerosol loading was located at SB, which is related to the special geographical location that is easy for accumulation of pollutants (Andrews et al., 2016). There was no notable increasing or decreasing trends in southwest China. Stations over YRD have persistent trends over the period study. AOD in SB has decreased after 1980 until the last period and continuous decreasing trends is also occurred over PRD during the last two periods. AOD in YRD exceeds all other regions from 1991, while mean AOD values in central China and SB are the second and third highest (See Table 1).

5. Discussion

In this research, the performance of visibility for analyzing the variability of AOD was evaluated and new algorithm was developed to retrieve AOD. However, there are some limitations in the KM-Elterman algorithm. The MODIS data were used as the reference to calculate new parameters. However, MODIS datasets still have some uncertainties (Zhang and Reid, 2009; Zhang et al., 2016b). Thus, more accurate AOD data should be used and applied to the new algorithm in the future work.

To evaluate the representativeness of visibility for analyzing AOD, linear interpolation was applied to fill data gaps. This interpolation method may induce some biases in the analysis between visibility and AOD. According to Zhang et al. (2016b) and Li et al. (2013), the interpolation method may not have a strong influence on the regional analysis of AOD, especially when the percentage of missing data is less than 10%. This study adopted the SVD method, which can separate the domain modes. Since only the first two

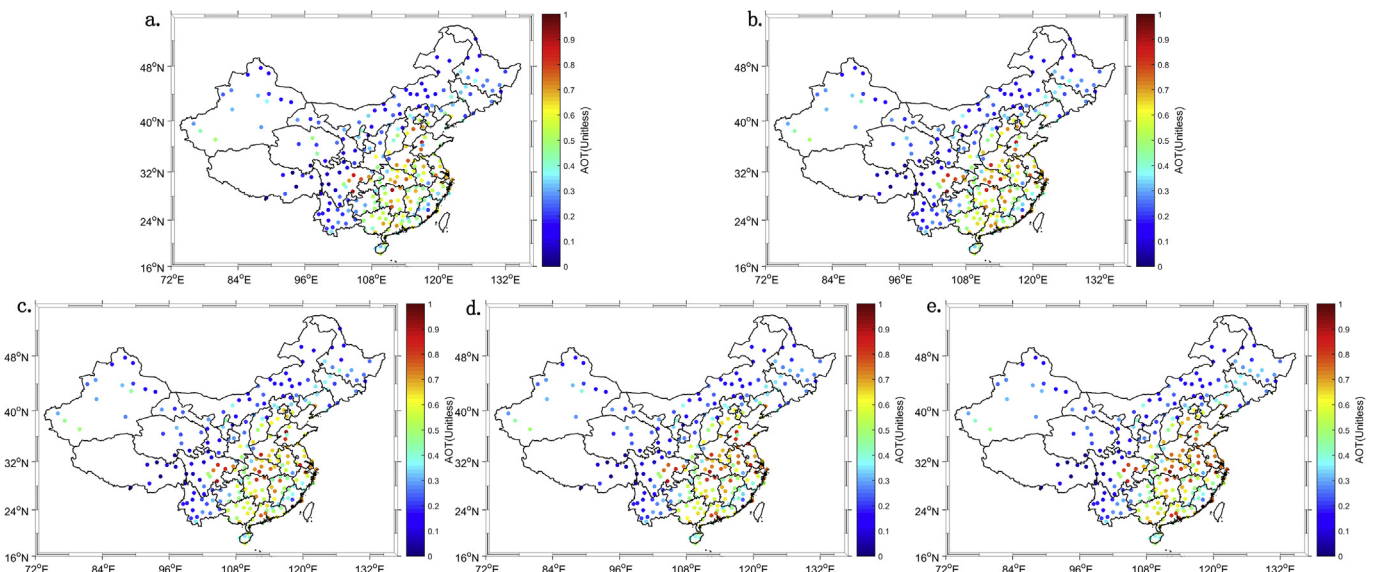


Fig. 9. Spatial distribution of mean inferred AOD during 1973–1980, 1981–1988, 1989–1996, 1997–2004, and 2005–2014.

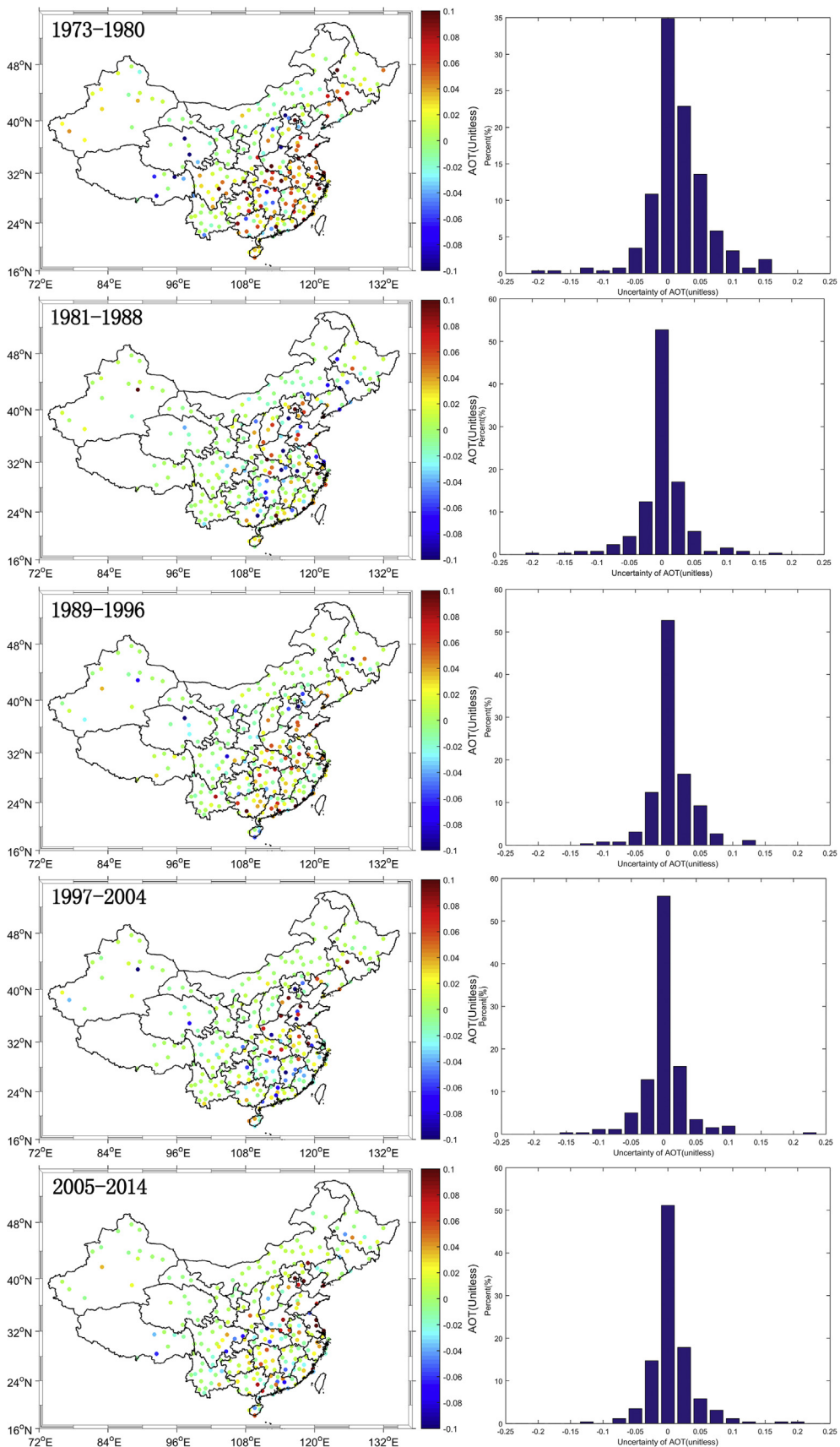


Fig. 10. Variability of inferred AOD during 1973–1980, 1981–1988, 1989–1996, 1997–2004, and 2005–2014 for all stations.

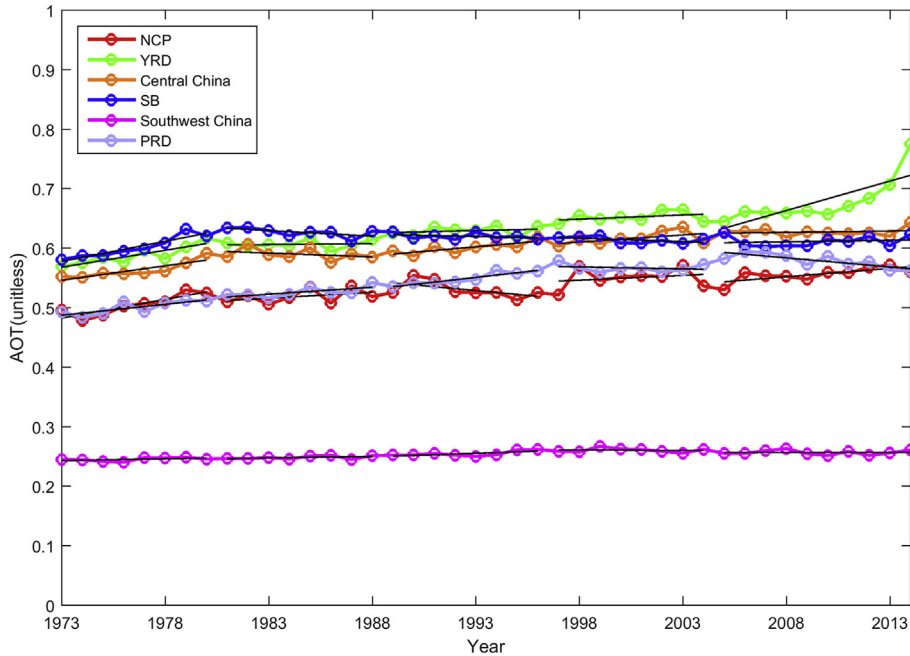


Fig. 11. Annual inferred AOD from 1973 to 2014 in the selected regions.

Table 1

AOD trends (/decade) over North China Plain (NCP), Yangtze River Delta (YRD), central China, Sichuan Basin (SB), southwest China, and Pearl River Delta (PRD) during five periods.

Regions	1973–1980	1981–1988	1989–1996	1997–2004	2005–2014
NCP	0.663	0.209	-0.342	0.169	0.301
YRD	0.598	0.033	0.085	0.148	1.069
Central China	0.509	-0.135	0.322	0.253	0.049
SB	0.711	-0.198	-0.079	-0.127	0.056
Southwest China	0.065	0.052	0.126	-0.016	0.00004
PRD	0.387	0.246	0.413	-0.069	-0.332

modes were investigated, the biases caused by the interpolation method can be ignored.

The used visibility measurements are observed by human and visibility meters (Ma and Yang, 2007). The uncertainty of visibility observed by human depends on the condition of observation and personal experience. Error of visibility recorded by visibility meter ranges from 10% to 20% (WMO, 1996). To evaluate the influence of uncertainty of visibility on the algorithm, the bias of visibility is assumed at 20%. Fig. 12 shows the histogram of relative difference of inferred AOD induced by uncertainties of visibility. Most of the errors are within ± 0.1 and the mean error induced by the visibility is about 0.04.

6. Conclusions

Visibility measurements are important indicator of historical aerosol loadings and have been observed by world meteorological stations for a long time. In this study, an improved method, KM-Elterman, was developed to retrieve Aerosol Optical Depth (AOD) from ground-based visibility. Parameters in the method were calculated based on MODIS Aqua (MYD04) AOD products during 2011–2014 for each station. New parameters were used to retrieve AOD during 1973–2010 and the performance of inferred AOD data was evaluated by MYD04 AOD during 2002–2010. According to the scatter plots, the correlations between inferred AOD and MODIS AOD during 2002–2010 are 0.715 and 0.943 for monthly and

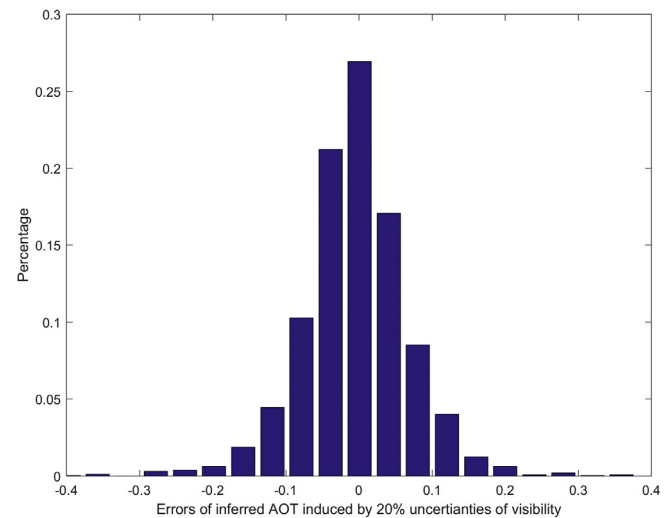


Fig. 12. Histogram of relative difference of inferred AOD induced by 20% uncertainties of visibility.

annual AOD, respectively. To examine the spatio-temporal performance of inferred AOD, SVD method was adopted. The first two modes of full dataset represent the seasonal AOD variability in North China Plain (NCP), southwest China, southeast coast, and

northwest China. The first three modes from the deseasonalized datasets represents inter-annual variations of AOD. Comparisons in spatial patterns and time series between MODIS AOD and inferred AOD indicated that inferred AOD were useful to investigate the aerosol variability and aerosol effects on climate change studies. Long-term AOD trends during 1973–2014 were investigated using the inferred AOD over China. High AOD (>0.5) during 1973–1980 were mostly concentrated in populated regions, such as North China Plain (NCP), Pearl River Delta (PRD), Sichuan Basin (SB), and central China. The number of stations with mean AOD value greater than 0.5 increased from 1973 to 2014. AOD trends in six regions were also analyzed in this study. Rapid growth of AOD was found during 1973–1980 in all regions, except southwest China. The inferred AOD in this study can better applied in studies of aerosol effects on climate change at a long-time scale.

Acknowledgments

This study was supported by the National Science Foundation of China (Grant No. 41572345). The author thanks NOAA for visibility data, GSFC/NASA for MODIS data.

References

- Andrews, E., Ogren, J., Kinne, S., Samset, B., 2016. Is there a bias in AERONET retrievals of aerosol light absorption at low AOD conditions? *Atmos. Chem. Phys. Discuss.* 2016, 1–43.
- Baumer, D., Vogel, B., Versick, S., Rinke, R., Mohler, O., Schnaiter, M., 2008. Relationship of visibility, aerosol optical thickness and aerosol size distribution in an ageing air mass over South-West Germany. *Atmos. Environ.* 42, 989–998.
- Boucher, O., Randall, A.D., Bretherton, P., Feingold, G., Forster, G., Kerminen, P., Kondo, V., Liao, Y., Lohmann, H., Rasch, U., 2013. Clouds and Aerosols in Climate Change 2013: The Physical Science Basis. Contribution of Working Group I to the Fifth Assessment Report of the Intergovernmental Panel on Climate Change. Cambridge University Press Cambridge, United Kingdom and New York, NY, USA.
- Che, H., Zhang, X.Y., Xia, X., Goloub, P., Holben, B., Zhao, H., Wang, Y., Zhang, X.C., Wang, H., Blarel, L., Damiri, B., Zhang, R., Deng, X., Ma, Y., Wang, T., Geng, F., Qi, B., Zhu, J., Yu, J., Chen, Q., Shi, G., 2015. Ground-based aerosol climatology of China: aerosol optical depths from the China Aerosol Remote Sensing Network (CARSNET) 2002–2013. *Atmos. Chem. Phys.* 15, 7619–7652.
- Elterman, L., 1970. Relationships between vertical attenuation and surface meteorological range. *Appl. Opt.* 9, 1804–1810.
- Field, C.B., Barros, V.R., Mach, K., Mastrandrea, M., 2014. Climate change 2014: impacts, adaptation, and vulnerability. Working Group II Contribution to the IPCC 5th Assessment Report-Technical Summary, pp. 1–76.
- Holben, B.N., Eck, T.F., Slutsker, I., Tanre, D., Buis, J.P., Setzer, A., Vermote, E., Reagan, J.A., Kaufman, Y.J., Nakajima, T., Lavenu, F., Jankowiak, I., Smirnov, A., 1998. AERONET - a federated instrument network and data archive for aerosol characterization. *Remote Sens. Environ.* 66, 1–16.
- Horvath, H., 1971. On the applicability of the koschmieder visibility formula. *Atmos. Environ.* 5, 177–184, 1967.
- Hsu, N.C., Si-Chee, T., King, M.D., Herman, J.R., 2004. Aerosol properties over bright-reflecting source regions. *Geoscience and Remote Sensing. IEEE Trans.* 42, 557–569.
- Huang, J., Chidong, Z., Joseph, M.P., 2009. African aerosol and large-scale precipitation variability over West Africa. *Environ. Res. Lett.* 4, 015006.
- Husar, R.B., Husar, J.D., Martin, L., 2000. Distribution of continental surface aerosol extinction based on visual range data. *Atmos. Environ.* 34, 5067–5078.
- Kaufman, Y.J., Koren, I., Remer, L.A., Rosenfeld, D., Rudich, Y., 2005. The effect of smoke, dust, and pollution aerosol on shallow cloud development over the Atlantic Ocean. *Proc. Natl. Acad. Sci. U. S. A.* 102, 11207–11212.
- Kessner, A.L., Wang, J., Levy, R.C., Colarco, P.R., 2013. Remote sensing of surface visibility from space: a look at the United States East Coast. *Atmos. Environ.* 81, 136–147.
- Klimont, Z., Smith, S.J., Cofala, J., 2013. The last decade of global anthropogenic sulfur dioxide: 2000–2011 emissions. *Environ. Res. Lett.* 8, 014003.
- Koschmieder, H., 1925. Theorie der horizontalen Sichtweite: Kontrast und Sichtweite. *Keim & Nemisch.*
- Lee, K.H., Wong, M.S., Kim, K., Park, S.S., 2014. Analytical approach to estimating aerosol extinction and visibility from satellite observations. *Atmos. Environ.* 91, 127–136.
- Levy, R.C., Mattoo, S., Munchak, L.A., Remer, L.A., Sayer, A.M., Patadia, F., Hsu, N.C., 2013. The Collection 6 MODIS aerosol products over land and ocean. *Atmos. Meas. Tech.* 6, 2989–3034.
- Levy, R.C., Remer, L.A., Kleidman, R.G., Mattoo, S., Ichoku, C., Kahn, R., Eck, T.F., 2010. Global evaluation of the Collection 5 MODIS dark-target aerosol products over land. *Atmos. Chem. Phys.* 10, 10399–10420.
- Li, J., Carlson, B.E., Lacis, A.A., 2013. Application of spectral analysis techniques in the intercomparison of aerosol data: 1. An EOF approach to analyze the spatial-temporal variability of aerosol optical depth using multiple remote sensing data sets. *J. Geophys. Res.-Atmos.* 118, 8640–8648.
- Li, Z., 2009. Toward understanding the climatic effects of aerosols under hazy environments: an overview of field observations in China. *AIP Conf. Proc.* 1100, 478–481.
- Lin, J.T., van Donkelaar, A., Xin, J.Y., Che, H.Z., Wang, Y.S., 2014. Clear-sky aerosol optical depth over East China estimated from visibility measurements and chemical transport modeling. *Atmos. Environ.* 95, 258–267.
- Luo, Y., Zheng, X., Zhao, T., Chen, J., 2014. A climatology of aerosol optical depth over China from recent 10 years of MODIS remote sensing data. *Int. J. Climatol.* 34, 863–870.
- Ma, S., Yang, Z., 2007. Specifications for Surface Meteorological Observation. China Meteorological Administration, Beijing, pp. 96–98.
- McClatchey, R.A., Fenn, R., Selby, J.A., Volz, F., Garing, J., 1972. Optical Properties of the Atmosphere. DTIC Document.
- Meyer, F.G., Curry, J.A., Brock, C.A., Radke, L.F., 1991. Springtime visibility in the Arctic. *J. Appl. Meteorol.* 30, 342–357.
- Ozkaynak, H., Schatz, A.D., Thurston, G.D., Isaacs, R.G., Husar, R.B., 1985. Relationships between aerosol extinction coefficients derived from airport visual range observations and alternative measures of airborne particle mass. *J. Air Pollut. Control Assoc.* 35, 1176–1185.
- Prohaska, J.T., 1976. A technique for analyzing the linear relationships between two meteorological fields. *Mon. Weather Rev.* 104, 1345–1353.
- Qin, S., Shi, G., Chen, L., Wang, B., Zhao, J., Yu, C., Yang, S., 2010. Long-term variation of aerosol optical depth in China based on meteorological horizontal visibility observations. *Chin. J. Atmos. Sci.* 34, 449–456.
- Qiu, J., Lin, Y., 2001. A parameterization model of aerosol optical depths in China. *Acta Meteorol. Sin.* 59, 368–372.
- Retalis, A., Hadjimitsis, D.G., Michaelides, S., Tymvios, F., Chrysoulakis, N., Clayton, C.R.I., Themistocleous, K., 2010. Comparison of aerosol optical thickness with in situ visibility data over Cyprus. *Nat. Hazards Earth Syst. Sci.* 10, 421–428.
- Sayer, A.M., Hsu, N.C., Bettenhausen, C., Jeong, M.J., 2013. Validation and uncertainty estimates for MODIS Collection 6 "Deep Blue" aerosol data. *J. Geophys. Res. Atmos.* 118, 7864–7872.
- Stocker, T., 2014. Climate Change 2013: the Physical Science Basis.
- WMO, 1996. WMO Guide to Meteorological Instruments and Methods of Observation.
- Wu, J., Luo, J., Zhang, L., Xia, L., Zhao, D., Tang, J., 2014. Improvement of aerosol optical depth retrieval using visibility data in China during the past 50 years. *J. Geophys. Res. Atmos.* 2014, JD021550.
- Yuan, C.-S., Lee, C.-G., Liu, S.-H., Chang, J.-c., Yuan, C., Yang, H.-Y., 2006. Correlation of atmospheric visibility with chemical composition of Kaohsiung aerosols. *Atmos. Res.* 82, 663–679.
- Zhang, J., Peng, G., Huang, M., Zhang, S., 2006. Are dust storm activities in North China related to Arctic ice–snow cover? *Glob. Planet. Change* 52, 225–230.
- Zhang, J., Reid, J.S., 2010. A decadal regional and global trend analysis of the aerosol optical depth using a data-assimilation grade over-water MODIS and Level 2 MISR aerosol products. *Atmos. Chem. Phys.* 10, 10949–10963.
- Zhang, J.L., Reid, J.S., 2009. An analysis of clear sky and contextual biases using an operational over-ocean MODIS aerosol product. *Geophys. Res. Lett.* 36, L15824.
- Zhang, Z.Y., Wong, M.S., 2017. A simplified method for retrieving aerosol optical thickness using visibility data between 1980 and 2014, a case study in China. *Ieee J-Stars PP* 1–8.
- Zhang, Z.Y., Wong, M.S., Lee, K.H., 2016a. Evaluation of the representativeness of ground-based visibility for analysing the spatial and temporal variability of aerosol optical thickness in China. *Atmos. Environ.* 147, 31–45.
- Zhang, Z.Y., Wong, M.S., Nichol, J., 2016b. Global trends of aerosol optical thickness using the ensemble empirical mode decomposition method. *Int. J. Climatol.* 36, 4358–4372.